Journal of Zhejiang University-SCIENCE A (Applied Physics & Engineering) 2025 26(5):456-470
www.jzus.zju.edu.cn; www.springer.com/journal/11582
E-mail: jzus_a@zju.edu.cn

Research Article

https://doi.org/10.1631/jzus.A2400097

Load-measurement method for floating offshore wind turbines based on a long short-term memory (LSTM) neural network

Yonggang LIN[1], Xiangheng FENG[1,2,3]✉, Hongwei LIU[1], Yong SUN[2,3]

[1]*State Key Laboratory of Fluid Power and Mechatronic Systems, Zhejiang University, Hangzhou 310058, China*
[2]*Windey Energy Technology Group Co., Ltd., Hangzhou 310012, China*
[3]*Zhejiang Key Laboratory of Wind Power Generation Technology, Hangzhou 310012, China*

Abstract: Complicated loads encountered by floating offshore wind turbines (FOWTs) in real sea conditions are crucial for future optimization of design, but obtaining data on them directly poses a challenge. To address this issue, we applied machine learning techniques to obtain hydrodynamic and aerodynamic loads of FOWTs by measuring platform motion responses and wave-elevation sequences. First, a computational fluid dynamics (CFD) simulation model of the floating platform was established based on the dynamic fluid body interaction technique and overset grid technology. Then, a long short-term memory (LSTM) neural network model was constructed and trained to learn the nonlinear relationship between the waves, platform-motion inputs, and hydrodynamic-load outputs. The optimal model was determined after analyzing the sensitivity of parameters such as sample characteristics, network layers, and neuron numbers. Subsequently, the effectiveness of the hydrodynamic load model was validated under different simulation conditions, and the aerodynamic load calculation was completed based on the D'Alembert principle. Finally, we built a hybrid-scale FOWT model, based on the software in the loop strategy, in which the wind turbine was replaced by an actuation system. Model tests were carried out in a wave basin and the results demonstrated that the root mean square errors of the hydrodynamic and aerodynamic load measurements were 4.20% and 10.68%, respectively.

Key words: Floating offshore wind turbine (FOWT); Long short-term memory (LSTM) neural network; Machine learning technique; Load measurement; Hybrid-scale model test

1 Introduction

As the world increasingly prioritizes renewable energy sources, wind energy has emerged as a prominent contender, offering a clean and sustainable alternative. Floating offshore wind turbines (FOWTs) represent an innovative technology in wind-energy utilization, and offer numerous advantages such as the ability to operate in deepwater regions, enhanced wind-energy harnessing potential, and minimal impact on marine ecosystems (Barooni et al., 2023). Consequently, they have become a focal point of research in the wind-energy industry. Unlike conventional fixed-base wind turbines, FOWTs encounter complicated load conditions in wind and wave environments (Micallef and Rezaeiha, 2021). Within a floating wind-turbine system, the rotor blades are subjected to aerodynamic loads induced by the wind, and the floating platform experiences hydrodynamic loads induced by waves and constraints from mooring line loads. Furthermore, platform motion in turn has complex coupled impacts on the load conditions of the FOWT (Yang C et al., 2023). Such complicated and coupled loads present significant challenges for platform structural design and safety control. Therefore, obtaining real operational data on these aerodynamic and hydrodynamic loads is of paramount importance for structural health assessment and cost-effective design optimization (Li et al., 2020).

The substantial aerodynamic and hydrodynamic loads on FOWTs, in addition to their huge size, make it challenging to measure these loads directly using traditional methods such as strain gauges and load cells (Li et al., 2020). Subsequent maintenance is also extremely difficult. According to the author's understanding,

✉ Xiangheng FENG, xiangheng_f97@zju.edu.cn
Yonggang LIN, https://orcid.org/0000-0001-5457-6388
Xiangheng FENG, https://orcid.org/0000-0002-0842-6044

Received Feb. 23, 2024; Revision accepted July 3, 2024; Crosschecked Apr. 2, 2025

there is a scarcity of literature on direct load measurements for large wind turbines and platforms. In the absence of real load data, researchers predominantly rely on numerical model simulations to acquire load data for structural design. Presently, approaches for calculating aerodynamic loads based on blade-element momentum theory and calculation of hydrodynamic loads based on potential flow theory heavily rely on empirical formulas and hypotheses, leading to certain deficiencies in calculation accuracy (Feng et al., 2023a). On the other hand, computational fluid dynamics (CFD) methods, which offer higher calculation accuracy, incur high time costs and are not suitable for real-time load measurement or calculation. Consequently, there has been a growing focus on model-based indirect load-measurement methods. Pahn et al. (2017) developed the inverse load model of a 5 MW fixed offshore wind turbine (OWT). The dynamic and static thrust measurements were achieved by measuring the tower's acceleration and strains. Maes et al. (2016) evaluated the tower load of a monopile OWT based on acceleration and stress signals and compared the effects of several filter algorithms. However, the influence of wind load was not taken into account. Song et al. (2022) used acceleration data and strain data to predict the wind loads on the offshore FINO3 platform with an extended Kalman filter algorithm (though wave-load effects were neglected). Currently, the available literature regarding indirect load-measurement methods for FOWTs in wind and wave conditions remains sparse, as it involves highly complicated and nonlinearly coupled aero-hydrodynamic characteristics (Dai et al., 2018; Wen et al., 2018; Chen et al., 2019), making the load identification through mathematical models difficult.

Machine learning is a powerful nonlinear modeling technique which has achieved significant success in various engineering fields. Consequently, many scientists have begun to consider applying it to the area of FOWTs. By learning from a large amount of real or high-fidelity data, artificial neural network models can better capture the complex relationship between the marine environments and loads or responses of FOWTs, thereby improving prediction accuracy and reliability. Noppe et al. (2018) developed a neural network model utilizing wind speed, rotor speed, and blade-pitch angle as inputs to predict the axial thrust of the turbine. The model achieved an average error of less than 15% compared to actual strain measurements. Jiang et al. (2019) employed an extensive set of simulation data to construct a neural network model, outputting thrust based on wind speed, platform heave, and pitch-motion inputs. The study findings showed that the calculated thrust closely matched the reference, indicating a high level of consistency. Chen et al. (2021) proposed a SADA method based on artificial intelligence technology to predict the dynamic response of the Hywind floating wind turbine. This method intelligently and dynamically adjusted the numerical FOWT model by integrating the measured ocean environmental (wind and wave) data and platform motion data, leading to more accurate load calculation and tower-deformation prediction. Wang et al. (2022b) created a multi-layer perceptron neural network model that utilized the tower's acceleration and platform motion responses to predict the tower root loads; the root mean square error was approximately 5.4%. Ma et al. (2023) employed a long short-term memory (LSTM) neural network model to predict the mooring-line tension of a floating production, storage, and offloading (FPSO) unit and investigated the impact of factors such as time windows, grid layers, and neuron numbers on the model's accuracy. Yang Y et al. (2023) trained a reservoir computing (RC) machine learning model using platform-motion data from experimental results, and demonstrated its efficacy in predicting platform heave, sway, and pitch motion. Li et al. (2019) devised a neural network model with two perceptron layers, utilizing wave-height data to forecast the vertical load of a wave-energy buoy device, with a curve-fitting degree of 84.84%. This prediction result was subsequently applied for wave-energy control, yielding favorable control outcomes.

Currently, big-data training for aerodynamic loads relies on accurate wind-speed-distribution information within the rotor plane as well as operational data on the turbine (such as rotor speed and blade-pitch angle). In practical applications, measuring the entire plane's wind-speed field can be quite challenging, as it requires extremely reliable radar devices. Moreover, the sampling frequency of the wind turbine's operational data is typically too low (e.g. the supervisory control and data acquisition (SCADA) system's sampling frequency of 1 Hz) to meet the requirements for high-frequency aerodynamic load calculation (Noppe et al., 2018). Therefore, directly training aerodynamic load models often leads to computational accuracy issues.

Although there is considerable research on predicting the dynamic response of floating platforms, a machine learning modeling for hydrodynamic loads on floating offshore wind platforms is still in the exploratory stage. Due to the fluid memory effect, a moving floating wind turbine platform experiences radiation damping forces, which are determined by past platform motion (Roddier et al., 2010). Traditional simple multi-layer perceptron models often struggle to capture such load characteristics with historical memory effects. However, these load characteristics precisely align with the features of the LSTM neural network. Therefore, this paper introduces a novel method for measuring aerodynamic and hydrodynamic loads based on an LSTM neural network model. Initially, the LSTM hydrodynamic load model, with platform motion and wave states as input and hydrodynamic loads as output, was trained on high-fidelity data from CFD simulation results. Then, the aerodynamic loads on the wind turbine were computed with the D'Alembert principle. This approach circumvented the traditional challenges of directly measuring aerodynamic loads or training aerodynamic-load neural network models.

The content of this study is as follows: Section 1 introduces the current status of load-measurement techniques, Section 2 describes the load-measurement model, Section 3 details the establishment of the LSTM hydrodynamic load model, Section 4 covers the operational analysis of the load-measurement model, Section 5 discusses the application of the load-measurement method in the scaled model tests, and Section 6 provides a summary of this study.

2 Load-measurement model

2.1 Load-measurement method

In the complex marine environment, FOWTs are subject to the combined excitation of wind and wave loads, which mutually influence each other. Constrained by the mooring system, the platform encounters motion with six degrees of freedom (DOFs). Assuming that the FOWT is a rigid body, according to the D'Alembert principle, the dynamic equilibrium relationship can be expressed as follows:

$$\boldsymbol{F}_{\mathrm{Aero}}+\boldsymbol{F}_{\mathrm{Hydro}}+\boldsymbol{F}_{\mathrm{Moor}}+\boldsymbol{F}_{\mathrm{Inertia}}=\boldsymbol{0}. \tag{1}$$

The aerodynamic load $\boldsymbol{F}_{\mathrm{Aero}}$ and hydrodynamic load $\boldsymbol{F}_{\mathrm{Hydro}}$ can be regarded as the system's active forces, while the mooring load $\boldsymbol{F}_{\mathrm{Moor}}$ can be seen as the system's constraint force, and $\boldsymbol{F}_{\mathrm{Inertia}}$ represents the inertial force opposite to acceleration. At any given moment of rigid-body motion, the active force, constraint force, and inertial force constitute a balanced force system. The inertial force of the system can be directly calculated from the acceleration signal, and the mooring constraint force can be directly measured by load sensors or indirectly calculated from the platform-motion signals (Ren et al., 2022). Then, the remaining aerodynamic load and hydrodynamic load form a complementary relationship, so that knowing one leads to the knowledge of the other.

We proposed the novel load-measurement method (Fig. 1) to achieve a sequential calculation of hydrodynamic and aerodynamic loads. A well-trained neural network model is applied to calculate the platform's hydrodynamic loads based on the platform motion and wave-elevation signals in the sensor system. Simultaneously, the mooring-line loads and inertial loads can be measured or calculated based on the load cells and acceleration signals. Finally, the aerodynamic loads are calculated through the D'Alembert principle.

The hydrodynamic load can be obtained by integrating the hydrodynamic pressure on the platform. One can conclude easily that the hydrodynamic loads are closely related to the platform's geometry, wave conditions, and platform-motion states. Therefore, when constructing a neural network hydrodynamic load model with a known geometric shape, platform motion and wave conditions serve as model inputs. In this study, we primarily considered the case in which wind and waves align consistently and maintain a constant direction. Furthermore, only the surge and pitch DOFs were taken into account. Thus, the wave conditions could be directly described by the wave elevation collected by a wave gauge in front of the platform, and the platform-motion states could be described by the surge and pitch displacements, velocity, and acceleration signals collected by the kinematic measurement systems such as differential global positioning system (DGPS), real-time kinematic (RTK) system, and inertial navigation systems (INSs). The model output was the hydrodynamic loads aligned with the wave-propagation direction (i.e., the total force in the X direction).

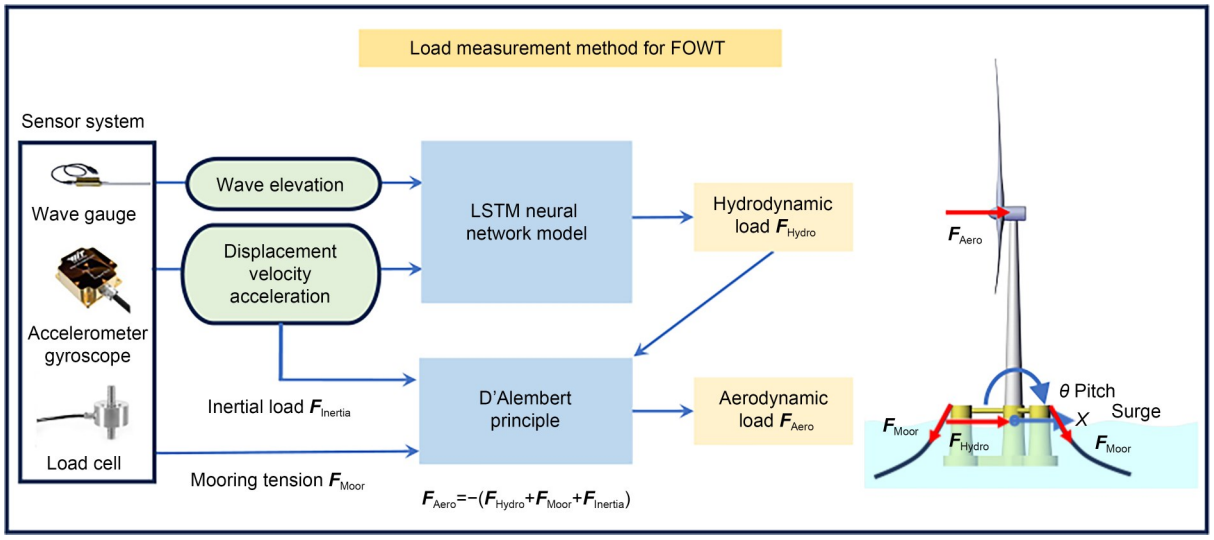

Fig. 1 Illustration of the load measurement method for FOWT

As one of the hydrodynamic load components, the radiation damping force is caused by the memory effect of the fluid and is obtained through the convolution calculation of the past platform motion. In other words, the radiation damping force at a given moment is determined by the platform motion at every past moment, with the influence of the motion from more distant moments diminishing over time. Such characteristics of load data precisely align with the features of LSTM neural network models, which can effectively remember and select past information.

2.2 Structure of the LSTM model

The LSTM neural network is a variant of recurrent neural networks (RNNs) and is widely used for processing and predicting time-series data such as text, audio, and video. Compared to traditional RNNs, the LSTM is designed with a special gating mechanism to address issues such as long-term dependencies, gradient explosion, and gradient vanishing (Wang et al., 2022a). These gating mechanisms enable LSTM to selectively remember or forget some information while maintaining and propagating important information over long periods. By learning the weights and biases of these gating mechanisms, LSTM can capture long-term dependencies within the data. The internal structure of an LSTM cell is illustrated in Fig. 2. The cell state c_t (t is the time, t=1, 2, ⋯, n) acts as a conveyor belt, transmitting information throughout the time-sequence process and allowing the addition or removal

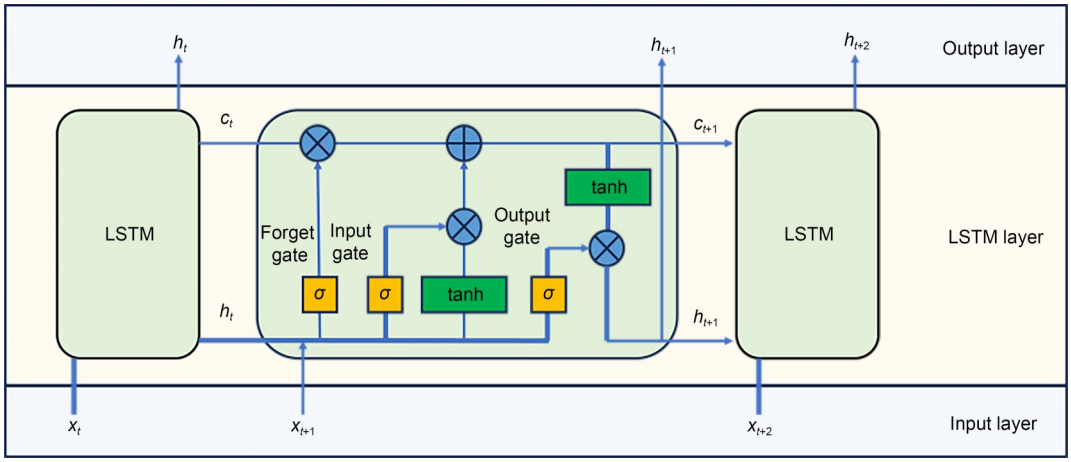

Fig. 2 Structure of an LSTM cell. x_t represents the input of the model at time t; σ is the function that determines whether the information in the cell state is forgotten

of information through input and forget gates. The output h_t is determined by the output gate and cell state. The relevant data-transmission equations for the LSTM neural network are detailed in Eqs. (S1)–(S7) of the electronic supplementary materials (ESM).

2.3 Model calculation process

In this study, we developed a sequence-to-sequence LSTM model to predict the hydrodynamic loads. The model inputs were wave elevation, acceleration, speed, and displacement of platform surge and pitch (sensitivity analysis of input dimensions will be discussed later). The process is illustrated in Fig. 3.

2.3.1 Sample data preparation

To accurately reflect the relationship between inputs and outputs, an elaborated CFD simulation model of the floating platform was created in STAR-CCM+ software. In addition, platform motion, wave elevation, and platform hydrodynamic loads under various conditions were extracted.

2.3.2 Sample data preprocessing

Data normalization was performed to address the significant differences in magnitude between input and output data.

2.3.3 Model creation and training

An appropriate model was constructed based on the characteristics of the sample data with initial parameters chosen from experience. Then, the model was trained iteratively until the best model parameters were determined.

2.3.4 Target load calculation

The trained LSTM model was employed to calculate the hydrodynamic loads based on "measured" input data. Then, the aerodynamic load calculation was conducted.

3 LSTM model construction

3.1 Data preparation

Currently, the majority of research on the hydrodynamics of floating offshore wind platforms relies on either the Morison formula (based on the empirical coefficients) or potential flow theory analysis methods (based on the inviscid assumption) (Liu et al., 2016). In contrast, the CFD method offers the advantage of considering fluid viscosity and all nonlinear physical effects, accurately describing the hydrodynamic loads,

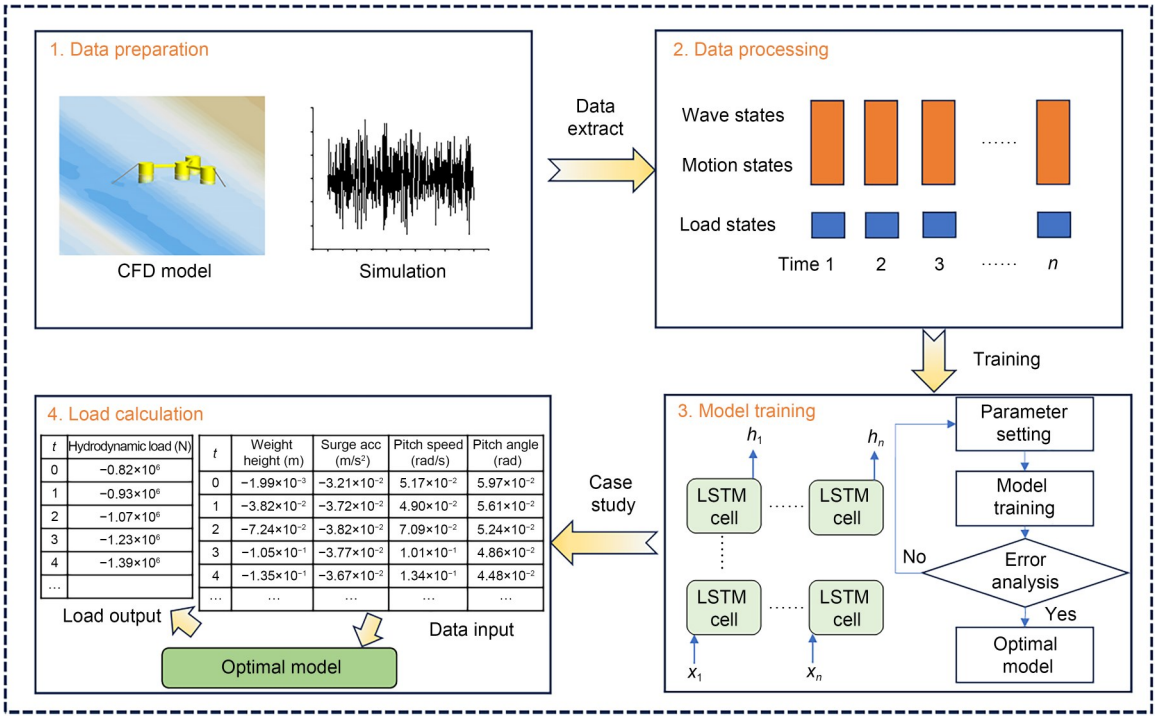

t	Hydrodynamic load (N)
0	−0.82×10⁶
1	−0.93×10⁶
2	−1.07×10⁶
3	−1.23×10⁶
4	−1.39×10⁶
…	

t	Weight height (m)	Surge acc (m/s²)	Pitch speed (rad/s)	Pitch angle (rad)
0	−1.99×10⁻³	−3.21×10⁻²	5.17×10⁻²	5.97×10⁻²
1	−3.82×10⁻²	−3.72×10⁻²	4.90×10⁻²	5.61×10⁻²
2	−7.24×10⁻²	−3.82×10⁻²	7.09×10⁻²	5.24×10⁻²
3	−1.05×10⁻¹	−3.77×10⁻²	1.01×10⁻¹	4.86×10⁻²
4	−1.35×10⁻¹	−3.67×10⁻²	1.34×10⁻¹	4.48×10⁻²
…	…	…	…	…

Fig. 3 Process of load-model calculation. Acc represents the acceleration

and effectively simulating the dynamic behavior of the floating platform under real marine conditions (Ciuriuc et al., 2022). Therefore, we employed STAR-CCM+ software to conduct the CFD simulation analysis and obtain accurate sample data.

3.1.1 Geometry model

The subject in this study was a 10 MW ZJUS10 semi-submersible floating wind turbine system, consisting of the wind turbine, floating platform, and mooring system. As the training sample data only focused on waves, platform motion, and platform hydrodynamic loads, only the floating platform and mooring system were considered in the CFD model in order to reduce simulation complexity. The influence of the wind turbine was substituted by the prescribed aerodynamic loads on the tower top. Even so, the parameters for the simulation model, such as mass, center of mass, and moments of inertia, were set to be the same as those of the whole system. The floating platform is depicted in Fig. 4. A detailed description can be found in Table S1 of the ESM.

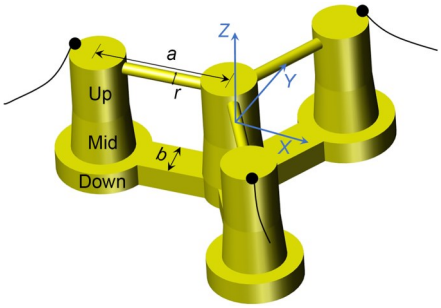

Fig. 4 The ZJUS10 semi-submersible floating platform. *a*, *r*, and *b* repressent the geometric lengths of the platform structure

3.1.2 CFD model

We constructed a numerical CFD model of the floating platform in STAR-CCM+ software. Dynamic fluid body interaction (DFBI) technology was adopted for fluid-field simulation under platform motion, as shown in Fig. 5. We applied the *k*-*ω* shear-stress transport (SST) turbulence model to close the Reynolds-averaged navier-stokes (RANS) equations, and established the volume of fluid (VOF) model to capture the

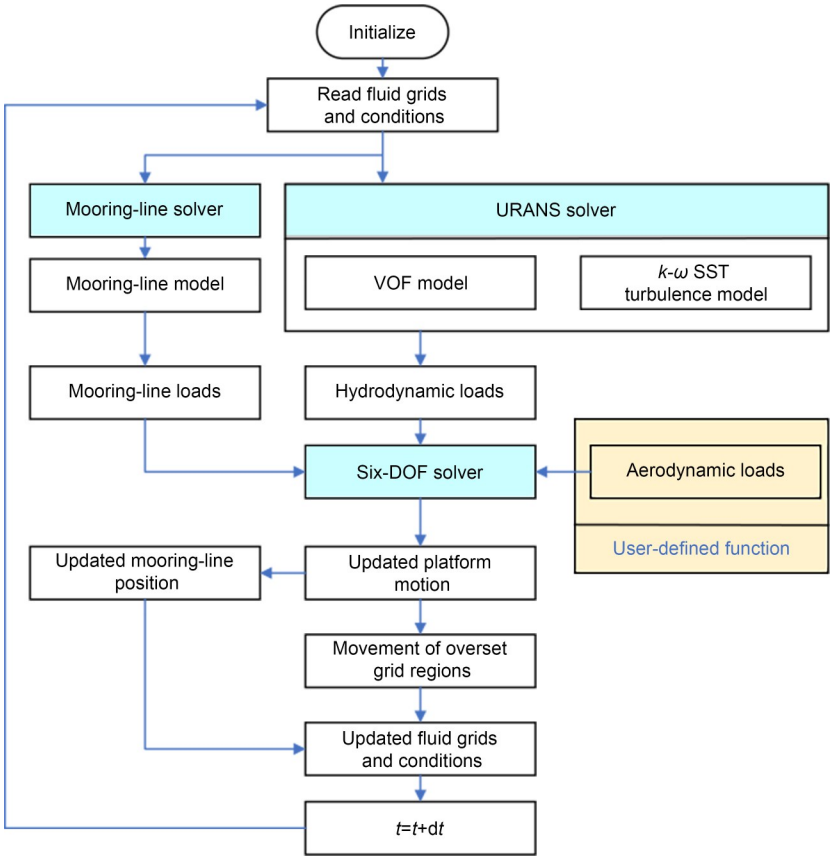

Fig. 5 DFBI calculation process. URANS represents the unsteady Reynolds-averaged navier-stokes

motion of the free surface. The piecewise extrapolating method (PEM) was applied to calculate the tensions of the three elastic and quasi-stationary catenaries, which were modeled by the catenary coupling element technique. In addition, we applied aerodynamic loads, precalculated by OpenFAST software, at the virtual hub position through the user-defined function. Under the excitation of aerodynamics loads, hydrodynamic loads, and mooring-line loads, the platform motion was calculated by the six-DOF solver using the Runge-Kutta method.

The entire fluid domain consisted of a background domain that described the wave motion and a motion domain that described the floating-platform motion. The data interaction between the two domains was achieved through overset grid technology, which is particularly suitable for complex motion. The background domain spanned a rectangular prism measuring 1500 m×1000 m×500 m, while the motion domain covered a rectangular prism measuring 200 m×200 m×100 m. The inlet boundary, upper boundary, and bottom boundary of the background domain were all set as velocity inlets, while the two sides of the background domain were set as symmetric planes and the outlet was set as a pressure outlet boundary. Additionally, a damping zone spanning two wavelengths was created at the outlet boundary to dissipate wave kinetic energy and minimize wave reflection. Fig. 6 shows the wave elevation at two different locations, where x_1 represents the wave zone in front of the platform and x_2 represents the damping zone far behind the platform. It was evident that the VOF model accurately reproduced wave results compared to theoretical values, and the damping zones effectively mitigated wave-particle motion. The validation of the mesh convergence and time-step convergence can be found in Section S3 of the ESM.

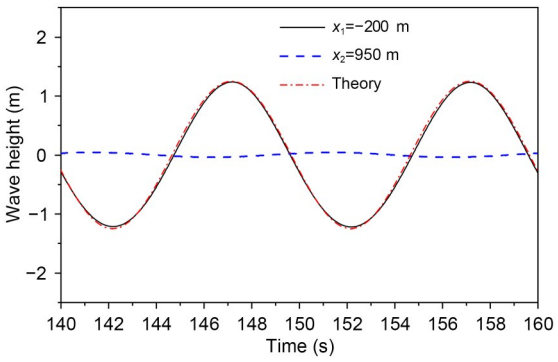

Fig. 6 Verification of the VOF model

3.1.3 Simulation analysis

The simulation results for the hydrodynamic loads along the *X*-axis direction in four different cases are plotted in Fig. 7. The dashed black line represents the hydrodynamic loads of a fixed platform with a regular wave height of 2.5 m and a period of 8.5 s, which exhibits a sinusoidal periodic variation. The solid black line indicates the loads of a floating platform under the same wave conditions, showcasing a noticeable reduction in amplitude which we attribute to platform motion. The red line signifies the hydrodynamic loads of the floating platform when subjected to both regular waves and wind loads. A comparison reveals that the presence of aerodynamic loads alters the periodic variation of hydrodynamic loads because it shifts the platform's equilibrium position, thereby altering the system's stiffness characteristics and the underwater platform shape. The blue line represents the hydrodynamic loads of the floating platform with an extremely irregular wave that has a significant height of 10.6 m and a peak period of 16.0 s, which demonstrates a substantial increase in amplitude variation. In summary, platform hydrodynamic loads are closely related to the wave conditions and platform motion, as mentioned before. Fig. 8 illustrates the distribution of the free surface

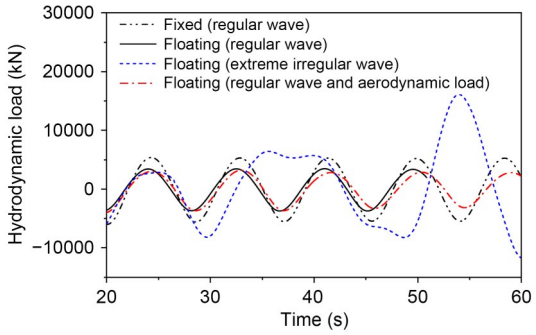

Fig. 7 Hydrodynamic load results for four cases

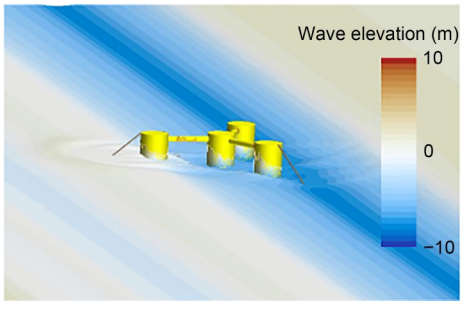

Fig. 8 Distribution of the wave elevation near the platform. References to color refer to the online version of this figure

in the case of irregular waves, and clearly shows the diffraction phenomenon that occurs when waves pass through the platform. Additionally, due to fluid viscosity, a small amount of fluid adheres to the platform surface. These phenomena are difficult to produce using traditional hydrodynamic calculation methods.

3.2 Data processing

The data on platform motion, wave height, and hydrodynamic loads are different in units and orders of magnitude. In order to ensure the accuracy and stability of the training process, the training data was preprocessed by regularization. We set the maximum and minimum values in the sample data as the upper and lower limits of the interval [0, 1], respectively, and the processing formula is as follows:

$$d_{\mathrm{p}} = (d - d_{\min}) / (d_{\max} - d_{\min}), \tag{2}$$

where d represents the original sample data; $d_{\min}$ and $d_{\max}$ represent the minimum and maximum values in the sample data, respectively; d_{p} represents the normalized data. This operation ensured that each sample data fell within the unit range and that there were no negative values. Correspondingly, after training the model to generate the output, a denormalization process was required for the data.

During the model training process, various statistical parameters were employed to evaluate learning performance. For a neural network model, the average-value error E_{mean}, extreme-value error $E_{\max}$, curve-fitting degree R_{fit}, and root mean square error E_{rms} are usually adopted. The detailed expression can be found in Section S4 of the ESM.

3.3 Determination of the optimal model

During the construction of the LSTM neural network model, it was important to avoid unreasonable model design, as this can lead to increased training time and poor fitting results. Neural network models typically have certain design spaces that allow for achieving the best fitting effect on the sample data by selecting appropriate model parameters. In this study, we determined the optimal model using the control variable method, in which each parameter of the model was adjusted individually while other parameters remained the same. The optimal model was considered to be reached when the error became stable without further reduction. Fig. 9 shows the determination process of the optimal model, which involved conducting sensitivity analyses on sample characteristics, model structure parameters, and training parameters in turn. The sample data used for training were generated from simulation results under a set of irregular sea conditions. The simulation time duration was 1 h, with 90% used for training and 10% used for verification. The initial model parameters were two LSTM layers and 64 neurons in each layer. The configuration of the workstation used for training the LSTM model is given in Table 1 and the detailed determination process can be found in Section S5 of the ESM.

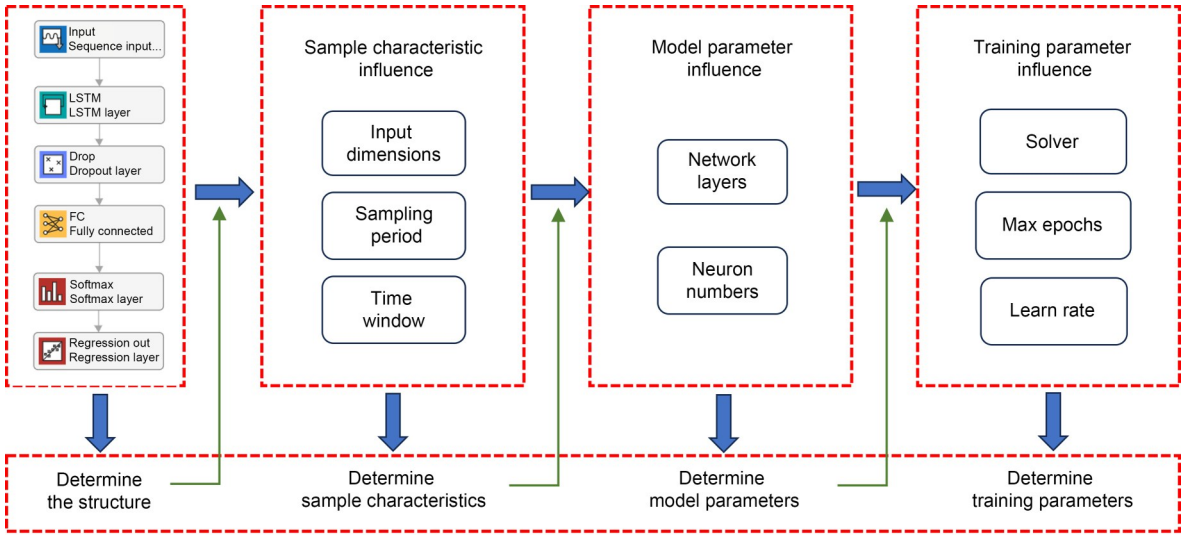

Fig. 9 Determination process of the optimal model

Table 1 Configuration of the workstation

Configuration	Description
CPU	Intel Xeon E5-2678
GPU	NVIDIA GeForce RTX 2060
RAM	256 GB
Parallel logic processor	64

4 Simulation verification

After identifying the optimal LSTM model, we further validated the effectiveness of the hydrodynamic load model in several simulated cases. The verification process was divided into two parts: verification in identical cases and verification in different cases. "Verification in identical cases" means that the training and verification data sets were all from simulation results obtained under the same sea-state conditions but at different time points. "Verification in different cases" refers to training and verification data sets from simulation results obtained under different sea-state conditions. After this stage, we carried out special-case and aerodynamic verification.

To accurately capture the internal relationship between wave elevation, platform motion state, and hydrodynamic load, we considered a variety of simulation cases based on the real sea conditions in the Gulf of Maine (Pegalajar-Jurado et al., 2018). These cases encompassed four wind conditions (low wind speed, rated wind speed, high wind speed, and extreme wind speed) and 16 irregular wave conditions, defined based on the significant wave height and peak period. Detailed simulation cases and the special case verification can be found in Sections S6 and S7 of the ESM.

4.1 Verification in identical cases

Under the same environmental conditions, sample data often exhibits a strong correlation. To validate the model, we carried out verifications for four designed cases which were most likely to represent the real operating sea state. Fig. 10 illustrates the model calculation results (red line) alongside ideal reference results (blue line), and the calculation errors are summarized in Table 2. It can be observed that the calculation curves closely align with the reference curves, with all curve-fitting degrees exceeding 94%. Of the four cases, the calculation result for case 64 demonstrated the highest fitting degree (98.43%) and the smallest E_{rms} (0.83%). In contrast, the prediction performance for case 22 was poorer, with the E_{rms} of 3.10%. This

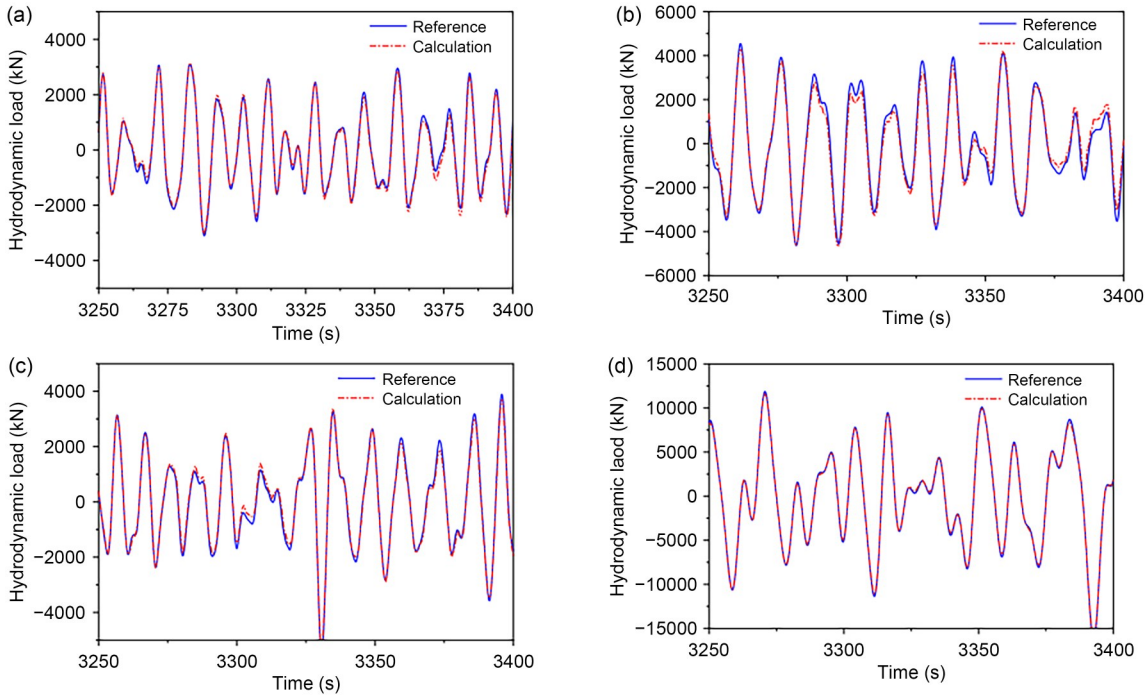

Fig. 10 Model verification for identical cases: (a) case 1; (b) case 22; (c) case 43; (d) case 64. References to color refer to the online version of this figure

Table 2 Model performance for verification in identical cases

Case	E_{mean} (%)	E_{max} (%)	R_{fit} (%)	E_{rms} (%)
1	0.74	3.03	95.41	2.71
22	1.51	4.77	94.29	3.10
43	0.72	3.10	95.30	2.54
64	0.10	1.51	98.43	0.83

discrepancy arose from the influence of aerodynamic loads. The aerodynamic loads reached the maximum in case 22, but dropped to near zero in extreme sea-state case 64. In the absence of aerodynamic loads, the hydrodynamic loads were solely determined by the wave height, as the platform motion was also determined by the wave. Therefore, the reason for the inferior calculation results in case 22 compared to case 64 was the neglect of certain motion states mentioned previously. Even so, the model's accuracy remained acceptable.

4.2 Verification in different cases

In order to assess the adaptability of the LSTM model across various operating conditions, we conducted a comprehensive analysis of model performance considering three environmental variables: wave height, period, and wind speed, as shown in Table 3. Validation under different operating conditions was categorized into two groups: a partially different group and a completely different group. A "partially different group" refers to the situations where the training and testing sets differed in one environmental variable while the others remained the same. A "completely different group" indicates that all environmental variables were entirely distinct.

All operating-condition data had a duration of 1 h. The comparison between the calculated and reference hydrodynamic loads is plotted in Fig. 11, and the model calculation error is summarized in Table 4. Two curves

Table 3 Verification cases

Verification type	Training case	Test case	Test condition		
			Wave height (m)	Wave period (s)	Wind speed (m/s)
Different wave heights	18, 22, 26, 30	65	3.04	8.5	11.4
Different wave periods	21–24	66	2.50	9.5	11.4
Different wind speeds	2, 18, 34, 50	67	2.50	8.5	13.9
Completely different	1–64	68	3.04	9.5	13.9

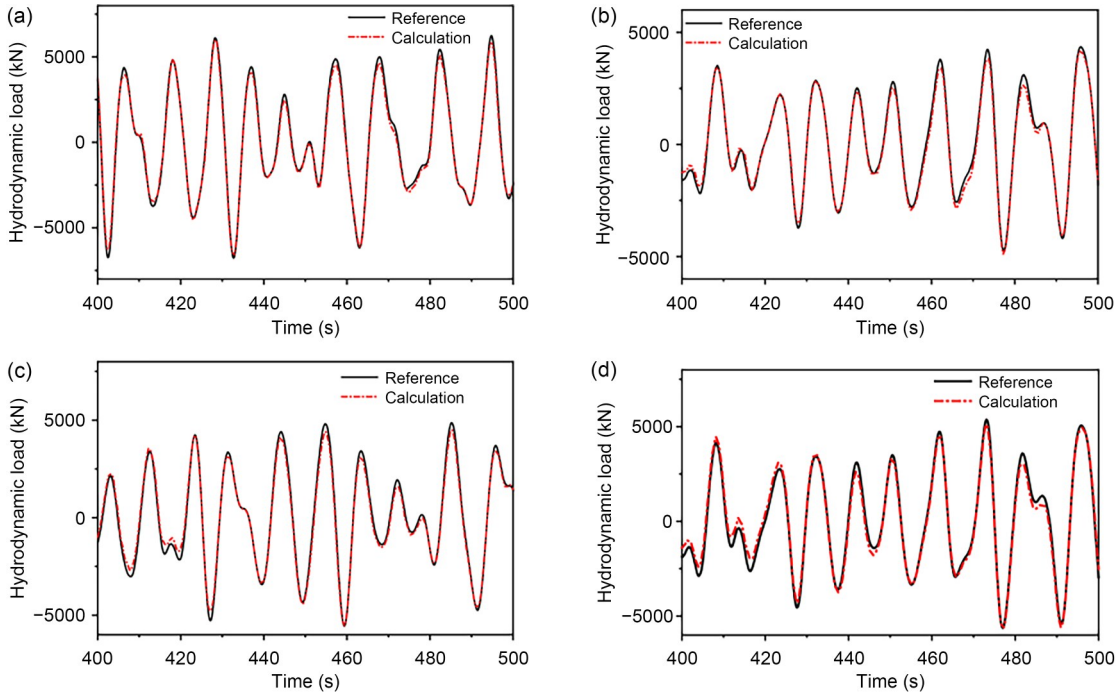

Fig. 11 Model verification in different cases: (a) different wave heights; (b) different wave periods; (c) different wind speeds; (d) completely different

Table 4 Model performance in verification in different cases

Case	E_{mean} (%)	E_{max} (%)	R_{fit} (%)	E_{rms} (%)
65	3.63	5.56	93.29	3.91
66	3.53	6.19	93.11	3.85
67	0.88	1.60	96.98	1.67
68	2.53	4.89	94.95	2.95

exhibited good consistency, with all curve-fitting degrees exceeding 93% and root mean square errors below 4%. However, these results were slightly inferior to those obtained in the verification in identical cases. Of the three variables, the model exhibited the best adaptation to wind speed, as this variable indirectly influenced hydrodynamic loads through platform motion. In case 68, the model calculation accuracy was overall better than those in case 65 and case 66, as there were more training samples, but lower than that in case 67, which involved more environmental variables. Overall, the model demonstrated the ability to adapt to different environmental conditions.

4.3 Aerodynamic verification

Once the hydrodynamic load calculation was completed, the axial aerodynamic loads F^x_{Aero} could be obtained using Eq. (3), which is as follows:

$$F^x_{Aero} = M\ddot{x} - F^x_{Hydro} - \sum T\cos\alpha\cos\beta, \tag{3}$$

where M is the mass of the FOWT; $\ddot{x}$ is the platform-acceleration signal; F^x_{Hydro} represents the axial hydrodynamic load calculated by the LSTM model; T signifies the mooring-line tension; α and β indicate the azimuth and inclination angles of the mooring line, respectively. Based on the hydrodynamic load calculation result for case 68, the aerodynamic loads calculated by the proposed method are depicted in Fig. 12, and the aerodynamic load calculation errors are recorded in Table 5. It is obvious that the variation frequency of aerodynamic loads was higher than that of hydrodynamic loads. The average-value error of 1.96%, the curve-fitting degree of 93.35%, and the root mean square error of 3.43% validate the effectiveness of the proposed load-measurement method to a considerable extent. For the simulation verification, the calculation error for aerodynamic loads primarily stemmed from the calculation error for hydrodynamic loads.

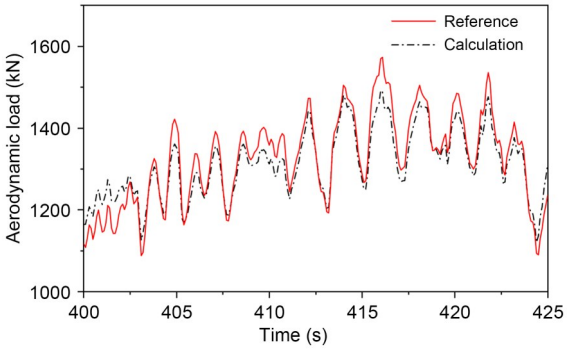

Fig. 12 Aerodynamic-load calculation results

Table 5 Model performance for aerodynamic verification

Parameter	Value
E_{mean} (%)	1.96
E_{max} (%)	2.15
R_{fit} (%)	93.35
E_{rms} (%)	3.43

5 Experimental verification

To further evaluate the validity of the proposed load-measurement method, we constructed a scale model of the 10 MW FOWT, and carried out two model tests in the wave basin at Zhoushan Campus of Zhejiang University, China.

5.1 Experimental setup

5.1.1 Experimental scheme

Froude number similarity was adopted to ensure the similarity of hydrodynamic characteristics. In order to overcome the aerodynamic similarity problem induced by the reduced Reynolds number, we propose a hybrid model strategy, as illustrated in Fig. 13. The physical wind turbine is replaced by the actuation system, whose goal is to generate the real-time aerodynamic loads calculated by the numerical software OpenFAST. For a more comprehensive understanding of the hybrid model, one can read our previous publication (Feng et al., 2023b).

5.1.2 Hybrid-scale model

Fig. 14 shows the 1∶50 scale model of the 10 MW FOWT, comprising the actuation system, tower, platform, and mooring lines. Ballast water was distributed inside the platform to ensure a designed draft depth. The sensor system mainly consisted of the environmental

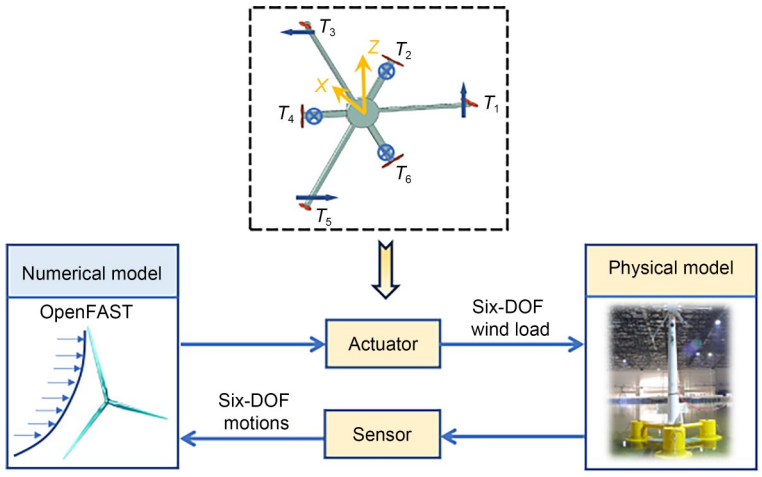

Fig. 13 Illustration of the hybrid model. T_1–T_6 represent the identifiers of the six fans

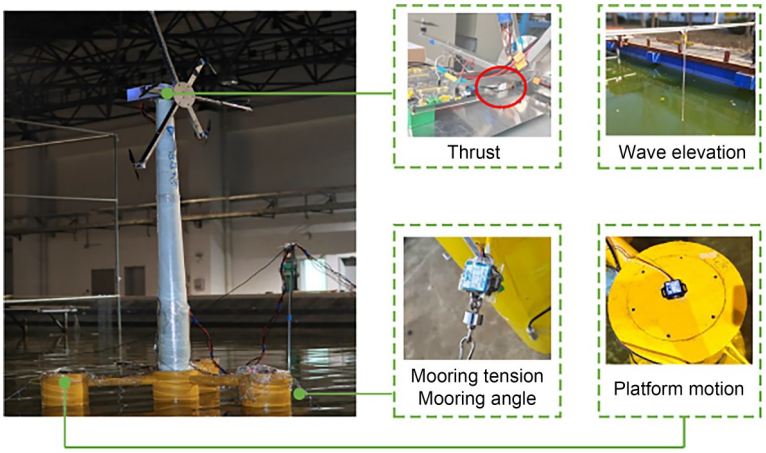

Fig. 14 Scale model and sensors

state measurement system (a wave-height meter), the load-measurement system including a tower-top thrust cell and mooring-line tension cells, and the platform-motion measurement system including an accelerometer and attitude sensors. All sensors were connected to the host computer with the Controller Area Network (CAN) communication protocol.

5.2 Results

Two experimental cases were considered in model testing to verify the performance of the load-measurement model under steady and unsteady conditions, as shown in Table 6. Exp. 1, which represents a steady case with uniform wind and regular waves, was mainly used to train the LSTM model and validate the hydrodynamic calculation. Exp. 2, which represents an unsteady case with turbulent wind and irregular waves, was mainly used to validate the aerodynamic calculation. One should keep in mind that the LSTM model was trained by the model test data in consideration of differences between the simulation model and experimental model.

Table 6 Environmental conditions of the experimental cases

Case	Environmental type	Wind speed (m/s)	Wave height (m)	Wave period (s)
Exp. 1	Steady	11.4	2.5	8.5
Exp. 2	Unsteady	11.4	2.5	8.5

The load histories of the inertial load, constraint load, aerodynamic load, and hydrodynamic load in Exp. 1 can be found in Section S8 of the ESM. Figs. 15 and 16 show the wave height and platform motion, respectively. The platform oscillates around the equilibrium position, which is dominated by the wind load. The acceleration signal represents the values in the inertial coordinate system, obtained through

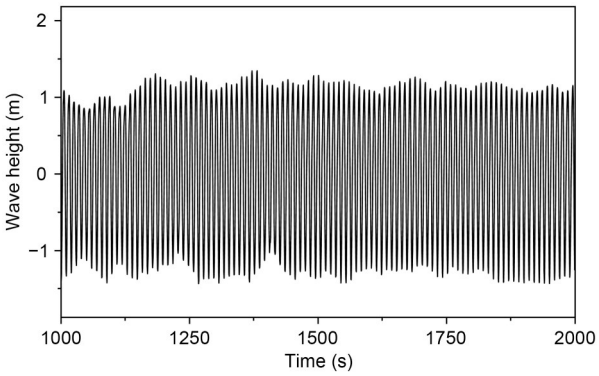

Fig. 15 Wave height sequences

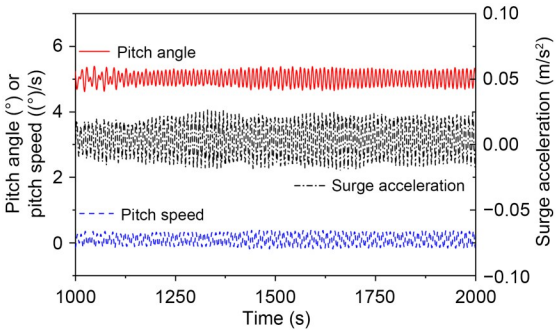

Fig. 16 Platform motion

coordinate transformation from the original body-fixed acceleration data. Fig. 17a shows the hydrodynamic load calculation results of the LSTM neural network model after training on experimental data. The calculation curve maintained good consistency with the reference one, with a curve-fitting degree of 95.57%. Fig. 17b shows the scatter diagram of the two loads. In general, the two lines are close enough to demonstrate good load-measurement accuracy. The root mean square error of the load calculation results was 2.54%.

The hydrodynamic load-measurement results for Exp. 2 are plotted in Fig. 18 and the load-measurement performance is displayed in Table 7. The error in Exp. 2 was clearly larger than that in Exp. 1 due to the influence of irregular waves. Compared to the simulation results, the experimental results from Exp. 2 exhibited lower accuracy, partly due to insufficient training data. In addition, the measurement error induced by the hardware influenced the model's calculation accuracy. Even so, the LSTM model exhibited good hydrodynamic load calculation ability. The comparison between the calculated aerodynamic load and the reference one is plotted in Fig. 19. The calculation results still closely followed the reference results. The extreme-value error was 5.89%; the average-value error was 0.88%; the root mean square error was 10.68%. It is worth noting that the calculation error for aerodynamic loads was higher than that for hydrodynamic loads. The disparity lies in the fact that the fluctuation range of the aerodynamic load is relatively small compared to that of the hydrodynamic load. Consequently,

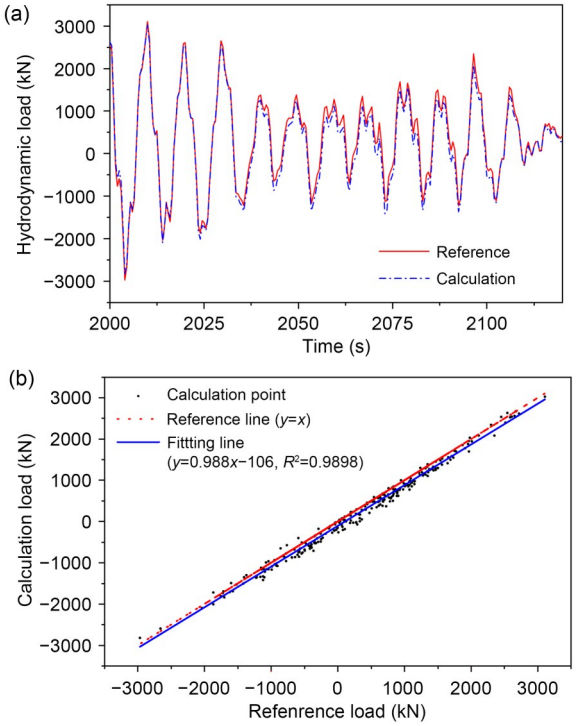

Fig. 17 Hydrodynamic load-measurement results for Exp. 1: (a) hydrodynamic load curve; (b) load scatter diagram

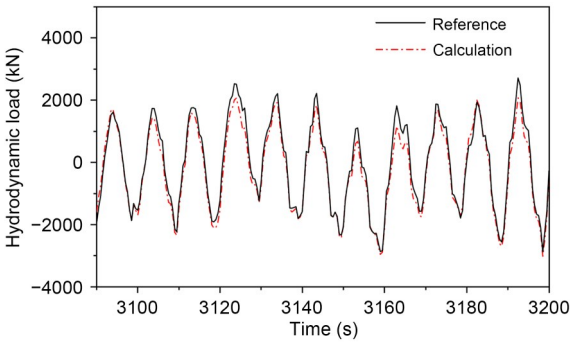

Fig. 18 Hydrodynamic load-measurement results from Exp. 2

Table 7 Load-measurement performance in model testing

Case	E_{mean} (%)	E_{max} (%)	R_{fit} (%)	E_{rms} (%)
F^x_{Hydro} in Exp. 1	1.83	1.30	95.57	2.54
F^x_{Hydro} in Exp. 2	2.00	2.83	92.44	4.20
F^x_{Aero} in Exp. 2	0.88	5.89	79.83	10.68

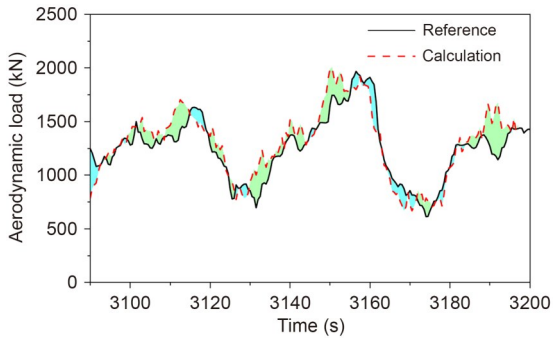

Fig. 19 Aerodynamic load-measurement results from Exp. 2

even minor relative errors in hydrodynamic load calculation can lead to significant errors in aerodynamic load calculation. When the error in the hydrodynamic load fluctuates sharply, the aerodynamic load calculation results may even fail to follow the trend of the reference values. To enhance the accuracy of aerodynamic load calculations, it is crucial to improve the precision of hydrodynamic load calculation. This can be achieved by increasing the amount of experimental training data and improving the quality of the experimental data. In general, engineers are more concerned about the overall measurement error during a period than the error at a certain time point. Therefore, an accurate assessment of the measurement error depends on the purpose of the load data (Pahn et al., 2017).

6 Conclusions

In this paper, we propose an aero-hydrodynamic load-measurement method for FOWT, based on the LSTM neural network model. First, we established a CFD simulation model of a floating platform, using DFBI and overset grid technologies. Then, we created and trained the LSTM model of hydrodynamic load calculation through platform motion and wave-elevation sequences, based on the simulation results. Finally, we verified the validity of the load model under various simulation conditions and with hybrid-scale model tests. The main conclusions are as follows:

1. The hydrodynamic load of the platform was closely related to wave states and platform-motion states. For the floating wind-power platform, we found that the optimal model structure for the LSTM neural network consisted of two layers, 128 neurons, and a time window of 1620 s.

2. The simulation verification results show that the LSTM model can accurately calculate the hydrodynamic loads of the platform, with the curve-fitting degree exceeding 93% and a root mean square error of less than 4%. For the aerodynamic load calculation, the average-value error is 1.96%; the extreme-value error is 2.15%; the curve-fitting degree is 93.35%; the root mean square error is 3.43%.

3. The experimental verification results show that the calculation accuracy in the experimental case is lower than in the simulation case. For the hydrodynamic load measurement, the curve-fitting degree is 92.44% and the root mean square error is 4.20%. For the aerodynamic load measurement, the curve-fitting degree is 79.83% and the root mean square error is 10.68%.

It is important to note that this study only considered the surge and pitch DOFs. Additionally, only surge acceleration, pitch speed, pitch angle, and wave elevation were selected as the model inputs. The ignorance of other platform motions will certainly import model errors. In the future, we envision this method being applied to actual full-scale FOWTs in real sea states. This would involve using more measurement equipment with high accuracy and high sampling frequency. Load-measurement accuracy would be improved by high-quality data and more input dimensions (up to 18 platform motion dimensions with displacement, speed, and acceleration in six DOFs).

Acknowledgments

This work is supported by the National Key Research and Development Program of China (No. 2023YFB4203000) and the National Natural Science Foundation of China (No. U22A20178).

Author contributions

Yonggang LIN designed the research. Xiangheng FENG processed the corresponding data and wrote the first draft of the manuscript. Hongwei LIU and Yong SUN revised and edited the final version.

Conflict of interest

Yonggang LIN, Xiangheng FENG, Hongwei LIU, and Yong SUN declare that they have no conflict of interest.

References

Barooni M, Ashuri T, Velioglu Sogut D, et al., 2023. Floating offshore wind turbines: current status and future prospects. *Energies*, 16(1):2. https://doi.org/10.3390/en16010002

Chen JH, Hu ZQ, Liu GL, et al., 2019. Coupled aero-hydro-servo-elastic methods for floating wind turbines. *Renewable Energy*, 130:139-153. https://doi.org/10.1016/j.renene.2018.06.060

Chen P, Jia CJ, Ng C, et al., 2021. Application of SADA method on full-scale measurement data for dynamic responses prediction of Hywind floating wind turbines. *Ocean Engineering*, 239:109814. https://doi.org/10.1016/j.oceaneng.2021.109814

Ciuriuc A, Rapha JI, Guanche R, et al., 2022. Digital tools for floating offshore wind turbines (FOWT): a state of the art. *Energy Reports*, 8:1207-1228. https://doi.org/10.1016/j.egyr.2021.12.034

Dai JC, Hu W, Yang X, et al., 2018. Modeling and investigation of load and motion characteristics of offshore floating wind turbines. *Ocean Engineering*, 159:187-200. https://doi.org/10.1016/j.oceaneng.2018.04.003

Feng XH, Fang JY, Lin YG, et al., 2023a. Coupled aero-hydro-mooring dynamic analysis of floating offshore wind turbine under blade pitch motion. *Physics of Fluids*, 35(4):045131. https://doi.org/10.1063/5.0141237

Feng XH, Lin YG, Gu YJ, et al., 2023b. Preliminary stability design method and hybrid experimental validation of a floating platform for 10MW wind turbine. *Ocean Engineering*, 285:115401. https://doi.org/10.1016/j.oceaneng.2023.115401

Jiang X, Day S, Clelland D, et al., 2019. Analysis and real-time prediction of the full-scale thrust for floating wind turbine based on artificial intelligence. *Ocean Engineering*, 175:207-216. https://doi.org/10.1016/j.oceaneng.2019.01.046

Li L, Gao Z, Yuan ZM, 2019. On the sensitivity and uncertainty of wave energy conversion with an artificial neural-network-based controller. *Ocean Engineering*, 183:282-293. https://doi.org/10.1016/j.oceaneng.2019.05.003

Li YJ, Li W, Liu HW, et al., 2020. Indirect load measurements for large floating horizontal-axis tidal current turbines. *Ocean Engineering*, 198:106945. https://doi.org/10.1016/j.oceaneng.2020.106945

Liu YC, Li SW, Yi Q, et al., 2016. Developments in semi-submersible floating foundations supporting wind turbines: a comprehensive review. *Renewable and Sustainable Energy Reviews*, 60:433-449. https://doi.org/10.1016/j.rser.2016.01.109

Ma G, Jin CL, Wang HW, et al., 2023. Study on dynamic tension estimation for the underwater soft yoke mooring system with LSTM-AM neural network. *Ocean Engineering*, 267:113287. https://doi.org/10.1016/j.oceaneng.2022.113287

Maes K, Iliopoulos A, Weijtjens W, et al., 2016. Dynamic strain estimation for fatigue assessment of an offshore monopile wind turbine using filtering and modal expansion algorithms. *Mechanical Systems and Signal Processing*, 76-77:592-611. https://doi.org/10.1016/j.ymssp.2016.01.004

Micallef D, Rezaeiha A, 2021. Floating offshore wind turbine aerodynamics: trends and future challenges. *Renewable and Sustainable Energy Reviews*, 152:111696. https://doi.org/10.1016/j.rser.2021.111696

Noppe N, Weijtjens W, Devriendt C, 2018. Modeling of quasi-static thrust load of wind turbines based on 1 s SCADA data. *Wind Energy Science*, 3(1):139-147. https://doi.org/10.5194/wes-3-139-2018

Pahn T, Rolfes R, Jonkman J, 2017. Inverse load calculation procedure for offshore wind turbines and application to a 5-MW wind turbine support structure. *Wind Energy*, 20(7):1171-1186. https://doi.org/10.1002/we.2088

Pegalajar-Jurado A, Bredmose H, Borg M, et al., 2018. State-of-the-art model for the LIFES50+ OO-Star wind floater semi 10 MW floating wind turbine. *Journal of Physics: Conference Series*, 1104:012024. https://doi.org/10.1088/1742-6596/1104/1/012024

Ren ZR, Zhou HY, Li BB, et al., 2022. Localization and topological observability analysis of a moored floating structure using mooring line tension measurements. *Ocean Engineering*, 266:112706. https://doi.org/10.1016/j.oceaneng.2022.112706

Roddier D, Cermelli C, Aubault A, et al., 2010. WindFloat: a floating foundation for offshore wind turbines. *Journal of Renewable and Sustainable Energy*, 2(3):33104. https://doi.org/10.1063/1.3435339

Song MM, Christensen S, Moaveni B, et al., 2022. Joint parameter-input estimation for virtual sensing on an offshore platform using output-only measurements. *Mechanical Systems and Signal Processing*, 170:108814. https://doi.org/10.1016/j.ymssp.2022.108814

Wang ZM, Qiao DS, Yan J, et al., 2022a. A new approach to predict dynamic mooring tension using LSTM neural network based on responses of floating structure. *Ocean Engineering*, 249:110905. https://doi.org/10.1016/j.oceaneng.2022.110905

Wang ZM, Qiao DS, Tang GQ, et al., 2022b. An identification method of floating wind turbine tower responses using deep learning technology in the monitoring system. *Ocean Engineering*, 261:112105. https://doi.org/10.1016/j.oceaneng.2022.112105

Wen BR, Dong XJ, Tian XL, et al., 2018. The power performance of an offshore floating wind turbine in platform pitching motion. *Energy*, 154:508-521. https://doi.org/10.1016/j.energy.2018.04.140

Yang C, Chen P, Cheng ZS, et al., 2023. Aerodynamic damping of a semi-submersible floating wind turbine: an analytical, numerical and experimental study. *Ocean Engineering*, 281:114826. https://doi.org/10.1016/j.oceaneng.2023.114826

Yang Y, Peng T, Liao SJ, 2023. Predicting 3-DoF motions of a moored barge by machine learning. *Journal of Ocean Engineering and Science*, 8(4):336-343. https://doi.org/10.1016/j.joes.2022.08.001

Electronic supplementary materials

Sections S1–S8, Tables S1–S13, Figs. S1–S6, Eqs. (S1)–(S11)